IET Power Electronics

Research Article

IET Journals
The Institution of Engineering and Technology

Design of *LCL* and *LLCL* filters for single-phase grid connected converters

ISSN 1755-4535
Received on 14th November 2015
Revised on 29th February 2016
Accepted on 15th April 2016
doi: 10.1049/iet-pel.2015.0922
www.ietdl.org

Majid Sanatkar-Chayjani, Mohammad Monfared ✉

Department of Electrical Engineering, Faculty of Engineering, Ferdowsi University of Mashhad, Mashhad, Iran
✉ *E-mail: m.monfared@um.ac.ir*

Abstract: Compared with the traditional *L* filters, the high order *LCL* and *LLCL* filters for grid integration of voltage source converters offer better switching harmonic attenuation even with smaller passive elements. However, the inherent resonance of the high order filters complicates the control of the converter and also the design of filter parameters, especially at presence of digital delays and grid impedance variations. This study proposes a simple design procedure for the *LCL* and the *LLCL* filters of a delay-based stabilised converter that satisfies the predefined constraints on the converter current ripple, grid current harmonics and the reactive power of the capacitor and at the same time, ensures adequate stability of the simple single loop current control against the resonance. Moreover, the effect of grid impedance on the filter performance and controller stability is taken into account, thus the proposed method is robust against a wide range of grid impedance variations. Experimental results for a 3 kW test rig under steady state and transient conditions confirm the effectiveness of the proposed filter design algorithm.

1 Introduction

The rapidly increasing energy demand and growing environmental concerns cause further attention to renewable energy sources (RESs). A current controlled voltage source converter (VSC) is an industrially accepted solution to interface the RES to power grid [1]. The quality of the current injected by VSCs to the utility grid is a main concern today. In order to prevent the harmonics and switching noises of the VSCs from penetrating the utility grid, some kind of passive low-pass filters, such as *L*, *LCL*, *LLCL* or other higher order filters are used in the output stage of the converter. The harmonic attenuation capability of *LCL* and *LLCL* filters are significantly higher than the traditional *L* filters, even with smaller passive elements, which offers lower volume, cost and losses [2]. Although, in spite of the prominent advantages of high order filters, the inherent resonance nature of them challenges the stability of the current control loop that may even lead to instability under certain circumstances. To deal with the resonance problem and stabilise the closed loop current control system, several methods are presented in recent studies [3–17]. Passive damping, using an additional resistor in the filter structure, is the simplest and most common method, which suffers from major drawbacks, such as power losses, reduced attenuation at switching frequencies and deteriorated performance when connected to a weak grid [3–5].

To ensure stability against the resonance and at the same time avoid additional losses, the active damping methods are proposed. In these methods, the resonance damping is achieved by modifying the control algorithm, which requires the addition of either some kind of digital filters to the control loop or extra sensors to the circuit [6–17]. Filter based methods include two distinct controllers in the current control loop. While the main controller regulates the low-frequency dynamics, the added one, which can be seen as a filter, attenuates the high-frequency resonances [6–9]. The grid impedance variations can weaken the damping effect and turn the stabilised system to instability. Active damping with extra control variables, such as the capacitor voltage [10, 11] or the capacitor current [12–17] are proposed. These techniques offer adequate damping in a selective way, at the cost of added circuit cost and control complexity, especially with considering digital implementation delays [16, 17].

An interesting technique to yield stability over a certain range of resonance to sampling frequency ratios, in a simple single-loop current control system is the delay-based stabilisation [15, 18–21]. In contrast to active damping solutions proposed yet, no digital filter is inserted in the current control loop and no extra variable, except the controlled current is sensed or controlled. In these approaches, different factors that influence the stability, considering the effect of the digital control delay are identified first. Then, the sampling and/or the resonance frequency are carefully selected such that adequate stability margins are obtained for the single-loop control with a certain delay presented in the loop. For instance, considering the $1.5T_s$ delay, the grid current can be controlled directly without any passive or active damping method if the ratio of the resonance frequency to the sampling frequency lies between 1/6 and 1/2 (i.e. $1/6 < f_{res}/f_s < 1/2$). Other works are also available that change the total loop delay as another tuning factor, which lets a wider range for above ratio between the two frequencies. The nature of this damping characteristic caused by the delay is recently discussed in details by many authors [18–20]. Despite the advantages of low cost and simplicity of the control algorithm, the stability of these methods is highly affected by grid impedance variations. The change of grid impedance can push the resonance frequency outside the stable region.

Regardless of the adopted stabilisation technique, designing the parameters of the high-order filters (*LCL* and *LLCL*) is also an important as well as complicated issue. In most of the previous works, the parameter design procedure is a trial and error method with the goal of size and cost reduction [22–27]. In this way, the *LCL* filter parameters are determined so that the converter-side inductor limits the converter current ripple, the capacitor value is simply chosen based on the reactive power limits and the grid-side inductor is decided to meet the grid current harmonic attenuation in accordance to IEEE-1547.2-2008 standard [28]. A similar approach is also proposed for higher order filters, such as the *LLCL* [24], the *LTCL* [25] and the *LCL-LC* filters [26].

In combination with the delay-based stabilisation methods, it is evidently difficult to find the best compromise between various, sometimes conflicting, requirements of output current ripple, harmonic attenuation, reactive power limits, size of components and the stability margins. Consequently, this paper proposes a simple design procedure for the *LCL* and the *LLCL* filters of a

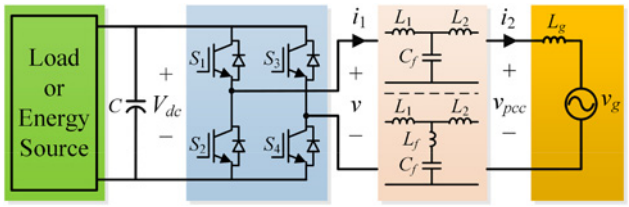

Fig. 1 *Grid-connected single phase VSC*

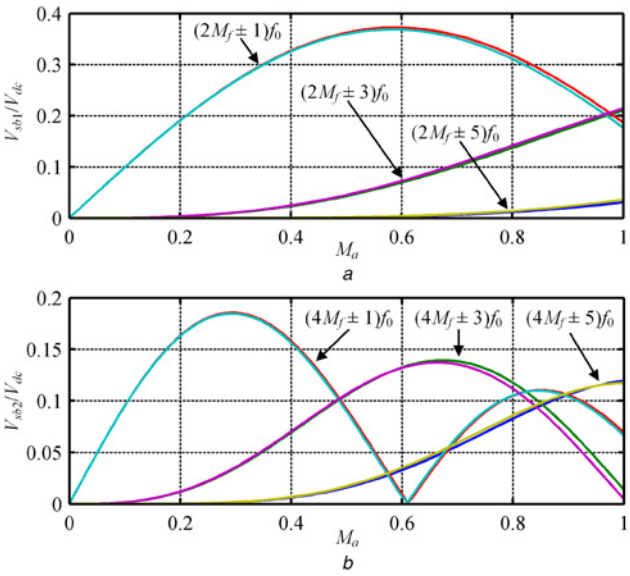

Fig. 2 *Normalised harmonics amplitudes of the VSC output voltage*

a First sideband
b Second sideband

delay-based stabilised converter that ensures stability of the closed loop system, and at the same time meets the reactive power, current ripple and harmonic limits requirements. The effect of grid impedance variations on the system stability is also considered, which ensures robust operation even with a weak grid.

The rest of the paper is organised as follows: Section 2 formulates the switching harmonics of the single phase converter with the unipolar asymmetrical modulation. In Section 3, the characteristics of the *LCL* and the *LLCL* filters in both low and high frequency ranges are investigated. In Section 4, the single loop current control of the converter system, with delay-based stabilisation is explained. The step by step design procedure for both *LCL* and *LLCL* filters is presented in Section 5. The experimental results are given in Section 6 and Section 7 concludes the paper.

2 Harmonics in the output of the single phase VSC

The power stage of the grid-connected single phase VSC is shown in Fig. 1. The switching harmonics of the VSC output voltage v appear in the grid current. As mentioned before, to adequately suppress the switching harmonics in the current, the VSC is connected to the grid through a high-order low-pass *LCL* or *LLCL* filter.

The most common modulation method for the single phase VSC is the unipolar asymmetrical (double-update) regular sampled pulse-width modulation (PWM), for which the output voltage of the VSC is expressed as [29] (see (1))

where $q = 2\,m + (2n-1)/M_f$ and V_{dc} is the dc link voltage, M_a and M_f are the amplitude and the frequency modulation indices, respectively, ω_c and ω_0 are the carrier and the fundamental frequencies, respectively, $(M_f = \omega_c/\omega_0)$ and $J_n(x)$ is the integral of Bessel function, which is expressed as $J_n(x) = \int_0^{\pi} \cos(n\pi - x\sin\tau)\,d\tau$. In the asymmetrical unipolar PWM, the sampling frequency is $\omega_s = 2\omega_c$ and obviously, the first sideband is located at $2\omega_c$.

From (1), the amplitude of the high frequency switching components (i.e. sideband harmonics) can be derived as (2). The two first sidebands are plotted in Fig. 2.

$$\underset{\substack{m=1,2,\ldots,\infty \\ n=\pm1,\pm2,\ldots,\pm\infty}}{V_{\mathrm{sb},m}(n)} = \frac{4V_{\mathrm{dc}}}{\pi}\frac{1}{q}J_{2n-1}\left(q\frac{\pi}{2}M_{\mathrm{a}}\right)\cos\left([m+n-1]\pi\right) \quad (2)$$

The lower the frequency of the sideband, the greater the harmonic amplitude; that is, the most dominant harmonics, as demonstrated in Fig. 2, are located around the first and the second sidebands.

3 *LCL* and *LLCL* filters characteristics

Both *LCL* and *LLCL* filters are shown in Fig. 1. The transfer functions of the converter voltage (v) to the converter and grid currents (i_1 and i_2) for the *LLCL* filter are formulated as [24]

$$\begin{cases} Y_{11}(s) = \dfrac{i_1(s)}{v(s)} = \dfrac{C_f(L_2' + L_f)s^2 + 1}{C_f[L_1L_2' + (L_1 + L_2')L_f]s^3 + (L_1 + L_2')s} \\ Y_{21}(s) = \dfrac{i_2(s)}{v(s)} = \dfrac{C_fL_fs^2 + 1}{C_f[L_1L_2' + (L_1 + L_2')L_f]s^3 + (L_1 + L_2')s} \end{cases} \quad (3)$$

where $L_2' = L_2 + L_g$ and L_g represents the equivalent inductance of the grid. Apparent from (3), the resonance frequency of the *LLCL* filter is $\omega_{res} = [(L_1 + L_2')/(C_f \quad (L_1L_2' + L_1L_f + L_2'L_f))]^{1/2}$. The transfer functions for the *LCL* case can be readily derived by setting L_f equal to zero. The transfer functions Y_{11} and Y_{21} determine the filter attenuation for i_1 and i_2 currents, respectively. Fig. 3 shows the Bode plots of Y_{21} for the *LCL* and the *LLCL* filters.

As it can be seen in Fig. 3 and presented in (4), the *LCL* filter offers a high attenuation at high frequencies, where the gain rolls-off at −60 dB/decade, while this rate is limited to −20 dB/decade for the *LLCL* case. However, the *LLCL* filter has a pair of complex-conjugate zeros in its transfer function located at the first sideband frequency (as the dominant switching harmonic). Therefore, the *LLCL* filter can significantly attenuate the first sideband harmonics. Although the high frequency roll-off rate of *LLCL* is the same as the *L* filter (with $L = L_1 + L_2'$), but the attenuation is higher with a factor of $1/(1 + L_1||L_2'/L_f)$.

$$\begin{cases} Y_{21,\mathrm{HF},LCL} = \left|Y_{21}(\mathrm{j}\omega)\right|_{\omega\gg\omega_{\mathrm{res}}} \cong \dfrac{1}{L_1L_2'C_f\omega^3} \\ Y_{21,\mathrm{HF},LLCL} = \left|Y_{21}(\mathrm{j}\omega)\right|_{\omega\gg\omega_{\mathrm{res}}} \cong \dfrac{1}{(L_1 + L_2')(1 + L_1||L_2'/L_f)\omega} \end{cases} \quad (4)$$

In the low frequency range, as calculated in (5) and shown in Fig. 3, the characteristics of both *LCL* and *LLCL* filters are identical and the same as a simple *L* filter with $L = L_1 + L_2'$. Therefore, the design of the current controller, regardless of the type of the filter, follows a

$$v(t) = \frac{4V_{\mathrm{dc}}}{\pi}\left\{\underbrace{\sum_{n=1}^{\infty}\frac{M_f}{n}J_n\left(n\frac{\pi}{2}\frac{M_a}{M_f}\right)\sin\left(n\frac{\pi}{2}\right)\cos\left(n\omega_0 t\right)}_{\text{fundamental component \& baseband harmonics}} + \underbrace{\sum_{m=1}^{\infty}\sum_{n=-\infty}^{\infty}\frac{1}{q}J_{2n-1}\left(q\frac{\pi}{2}M_a\right)\cos\left([m+n-1]\pi\right)\times\cos\left([2m\omega_c + (2n-1)\omega_0]t\right)}_{\text{sideband harmonics}}\right\} \quad (1)$$

IET Power Electron., 2016, Vol. 9, Iss. 9, pp. 1971–1978

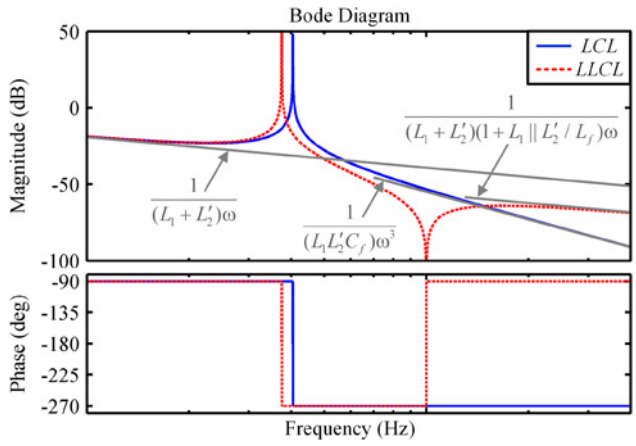

Fig. 3 *Bode plots of Y_{21} for the LCL and the LLCL filters*

similar procedure.

$$Y_{21,\mathrm{LF}} = \left|Y_{21}(\mathrm{j}\omega)\right|_{\omega \ll \omega_{\mathrm{res}}} \cong \frac{1}{(L_1 + L_2')\omega}. \tag{5}$$

Furthermore, the filters also present similar characteristics at high frequencies in terms of the converter current ripple attenuation, as presented in (6). As a result, regardless of the type of the filter, the converter current ripple is imposed only by the L_1 value.

$$\begin{aligned} Y_{11,\mathrm{HF}} &= \left|Y_{11}(\mathrm{j}\omega)\right|_{\omega \gg \omega_{\mathrm{res}}} \\ &\cong \frac{L_2' + L_{\mathrm{f}}}{[L_1 L_2' + (L_1 + L_2')L_{\mathrm{f}}]\omega}\bigg|_{L_{\mathrm{f}} \ll L_1, L_2'} \cong \frac{1}{L_1 \omega}. \end{aligned} \tag{6}$$

From the stability point of view, Bode plots of Fig. 3 show a sharp phase transition through $-\pi$ along with a high magnitude peak at the resonance frequency that readily leads to instability.

4 Single-loop control of grid current with delay-based stabilisation method

The proportional-resonant (PR) controller is commonly used to eliminate the steady-state error in the stationary reference frame. The open loop transfer function of the system, in presence of a delay T_{d}, can be derived as

$$G_{\mathrm{ol}}(s) = G_{\mathrm{PR}}(s) Y_{21}(s)\, \mathrm{e}^{-T_{\mathrm{d}} s} \tag{7}$$

where G_{PR} is the transfer function of the PR controller. Open loop Bode plots for both *LCL* and *LLCL* filters are shown in Fig. 4.

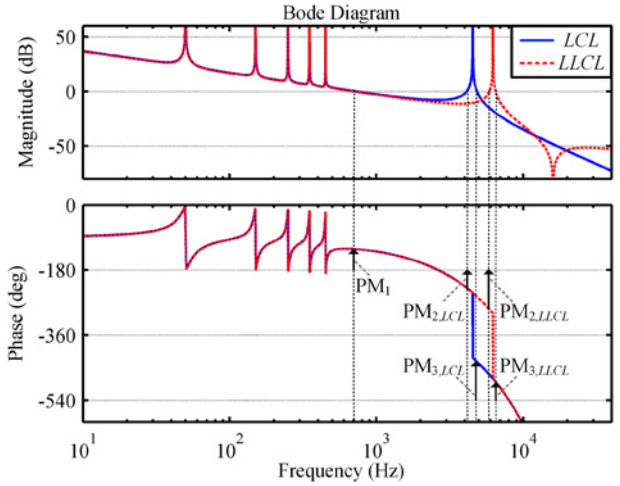

Fig. 4 *Open loop Bode plot of grid current loop for LCL and LLCL filters*

4.1 Stabilisation of the single-loop controller

A digitally implemented control system has several delays, mainly originated from the sampling, analogue-to-digital conversion and computations. All these can be modelled with one sampling period (T_{s}) delay. Taking into account the $0.5T_{\mathrm{s}}$ PWM transport delay of the converter system, a total delay of $T_{\mathrm{d}} = 1.5T_{\mathrm{s}}$ exists in the control loop [30]. The delay introduces a linear phase lag and changes the phase characteristic of open loop system. In delay-based stabilisation method, the resonance frequency (compared with the sampling one) is selected low enough to take benefit of this phase lag. This way, the phase lag originated from the loop delay causes the sharp phase change occurs below $-\pi$. If this sudden phase fall ends above -3π, then the single loop system remains stable. Based on this analysis, the stable range of resonance frequency for $T_{\mathrm{d}} = 1.5T_{\mathrm{s}}$ is already obtained as $f_{\mathrm{s}}/6 < f_{\mathrm{res}} < f_{\mathrm{s}}/2$ [18, 20].

Hence, Fig. 4 is plotted with the assumption that the resonance frequency is located in the stable rage of $f_{\mathrm{s}}/6 < f_{\mathrm{res}} < f_{\mathrm{s}}/2$; therefore, the sharp phase change lies between $-\pi$ and -3π. In this situation, three phase margins can be recognised. At the low frequency range, the phase margin PM_1 characterises the current control loop performance and is determined in the controller design stage, which is presented in the next subsection. Indeed, the dynamic performance of the closed loop system is imposed by the stability margin PM_1, while stability margins PM_2 and PM_3 have negligible effects on the dynamic performance and only must be positive to ensure the stability. In practice, PM_2 and PM_3 should be selected large enough to remain positive in presence of parameter uncertainties of the filter circuit and ensure stability against the

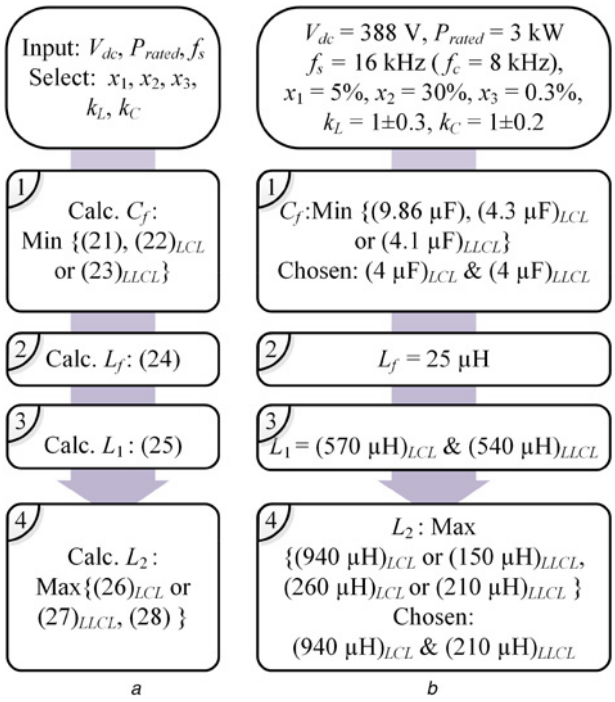

Fig. 5 *Four step design algorithm for the LCL and the LLCL filters*

a Design flow for the *LCL* and the *LLCL* filters
b Design example

resonance under all circumstances. The latter issue is fully attended in Section 5.

4.2 Tuning the controller parameters

As mentioned before, the characteristics of both *LCL* and *LLCL* filters at the low frequency range are identical and the same as a simple *L* filter with $L = L_1 + L_2$. Therefore, the PR controller for the current loop can be designed in the same way as for a system with the *L* filter. The tuning of PR constants is performed according to directions of [15]. Considering the negligible effect of the resonant terms of the PR controller on the gain crossover frequency, ω_{gc1} (for PM_1), then ω_{gc1} can be calculated as

$$\omega_{gc1} = \left(\pi/2 - PM_{1d}\right)/T_d \tag{8}$$

where PM_{1d} is the desired value for the PM_1 .To achieve the unity loop gain at the crossover frequency, the proportional gain is set to

$$k_p = \omega_{gc1}(L_1 + L_2). \tag{9}$$

The resonant gain is selected so that a negligible phase contribution at ω_{gc1} is achieved, i.e.

$$k_r = 0.02 k_p \omega_{gc1}. \tag{10}$$

5 *LCL* and *LLCL* filters design

Previous works have already proposed some criteria for selecting the parameters of high-order filters based on the limits on the current ripple of the inductors and the reactive power of the capacitor while the stability against the resonance is achieved with a passive or active damping method [22–26]. In this paper, the tuning of filter parameters is conducted in conjunction with the delay-based stabilisation technique. Indeed, the proposed step-by-step filter design algorithm satisfies the predefined constraints on the converter current ripple, grid current harmonics and the reactive power of the capacitor and at the same time, ensures adequate stability of the simple single loop current controller. Moreover, the effect of grid impedance on the filter performance and controller stability is taken into account, thus the proposed method is robust against a wide range of grid impedance variations.

In the following, the limits on the converter current ripple, the grid current harmonics and the reactive power are first presented, then the stability constraints of the closed-loop system are derived and finally a simple and systematic procedure to design the filter parameters is presented to simultaneously meet all the constraints.

5.1 Limits on the converter current ripple, the grid current harmonics and the reactive power of the filter capacitor

To design the parameters of a *LCL* or *LLCL* filter, some limits on current ripples and harmonics and reactive power should be considered, which are already discussed in [22, 24, 25]:

i. At the fundamental frequency, both filters act as a shunt capacitor that supplies reactive power. The reactive power by capacitor must be limited to a per cent, we call it x_1, of the rated power (generally $x_1 = 2.5$ to 5%).

ii. The converter side current ripple mainly determines the current rating of converter switches and is decided to be a per cent, we call it x_2, of the peak rated current of the converter $I_{P,rated}$ (generally $x_2 = 15$ to 40% [24]). In both cases, the maximum current ripple can be derived as [24]

$$\left(\Delta i_{1,max} = \frac{V_{dc} T_s}{8 L_1}\right) \le x_2 I_{P,rated}. \tag{11}$$

iii. The IEEE-1547.2-2008 standard recommend that all harmonics higher than 35th in the grid current must be lower than a per cent, $x_3 = 0.3\%$, of the rated current. To address the above requirement, as already discussed in Section 3, in the case of an *LCL* filter, the first sideband and in the case of an *LLCL* filter, the second sideband must be limited as

$$\begin{cases} \left(i_{2,sb1,max} = Y_{21,HF,LCL} V_{sb1,max}\right) \le x_3 I_{P,rated} \\ \left(i_{2,sb2,max} = Y_{21,HF,LLCL} V_{sb2,max}\right) \le x_3 I_{P,rated} \end{cases} \tag{12}$$

where the $V_{sb1,max}$ and $V_{sb2,max}$ are the maximum values of all sideband amplitudes in the expected range of variations for M_a, which can be replaced from (2) or readily from Fig. 2.

5.2 Constraints for stability against the resonance

However by setting the resonance frequency in accordance to $f_s/6 < f_{res} < f_s/2$ (sharp phase change occurs between $-\pi$ and -3π) the stability of single-loop current regulator is achieved, but sufficient damping at resonance frequency, in terms of the phase margins PM_2 and PM_3, must be provided to ensure positive margins under the expected range of filter parameter uncertainties. In a weak grid, the grid impedance variations lead to a wide uncertain range of the resonance frequency that must be also explored. Therefore, according to the grid impedance condition, the expected range of variation of resonance frequency should be first determined, then the filter parameters must be chosen such that the resonance frequency range always remains inside the stable range of $f_s/6 < f_{res} < f_s/2$ with appropriate margins.

In the case of a PR controller, where the phase change due to the resonance network just affects the low frequencies (obvious in Fig. 4), then the open-loop system phase in vicinity of the resonance frequency can be assumed as

$$\measuredangle G_{ol}(j\omega) = \begin{cases} -\pi/2 - \omega T_d & \omega < \omega_{res} \\ -3\pi/2 - \omega T_d & \omega > \omega_{res} \end{cases}. \tag{13}$$

As it can be seen in Fig. 4, the gain crossover frequencies for PM_2 and PM_3 are slightly lower and higher than the resonance frequency, respectively. With a good approximation, both gain crossover frequencies can be replaced with the resonance frequency. Therefore, the criterion that the sharp phase change lies in the stable range of $-\pi$ to -3π, with some margins as we already called PM_2 and PM_3, respectively, imposes that

$$\begin{cases} -\pi/2 - \omega_{res} T_d = -\pi - PM_2 \\ -3\pi/2 - \omega_{res} T_d = -3\pi + PM_3 \end{cases} \Rightarrow \begin{cases} PM_2 = -\pi/2 + \omega_{res} T_d \\ PM_3 = 3\pi/2 - \omega_{res} T_d \end{cases}. \tag{14}$$

Hence, the appropriate resonance frequency range that meets the desired phase margins PM_{2d} and PM_{3d} can be concluded as

$$\underbrace{\frac{\pi/2 + PM_{2d}}{T_d}}_{\omega_{min}} \le \omega_{res} \le \underbrace{\frac{3\pi/2 - PM_{3d}}{T_d}}_{\omega_{max}}. \tag{15}$$

It is worth mentioning that if one replace $PM_{2d} = PM_{3d} = 0$ and $T_d = 1.5T_s$, then (15) simplifies to $f_s/6 < f_{res} < f_s/2$.

On the other hand, the possible variation range for the resonance frequency with variation of L_g between zero and infinity can be

IET Power Electron., 2016, Vol. 9, Iss. 9, pp. 1971–1978

derived as

$$\underbrace{\sqrt{\frac{1}{(L_1+L_f)C_f}}}_{\omega_{res,\,min}} < \omega_{res} \le \underbrace{\sqrt{\frac{L_1+L_2}{[L_1L_2+(L_1+L_2)L_f]C_f}}}_{\omega_{res,\,max}}. \quad (16)$$

The resonance frequency decreases with the increase of L_g and vice versa. Therefore, based on (14) the minimum values for PM_2 and PM_3 occur for infinite and zero value of L_g, respectively. Consequently, in order to ensure that the resonance frequency range of (16) always lies within the stable range of (15), two stability constraints must be met

$$\frac{1}{(L_1+L_f)C_f} \ge \omega_{min}^2 \quad (17)$$

$$\frac{L_1+L_2}{[L_1L_2+(L_1+L_2)L_f]C_f} \le \omega_{max}^2. \quad (18)$$

In the case of the *LCL* filter, one must replace $L_f = 0$. Satisfaction of these two constraints guarantees the stability of the closed-loop system with sufficient phase margins while the grid impedance changes widely.

5.3 Choosing the proper phase margins

As mentioned before, the values of the PM_{2d} and PM_{3d} must be selected properly to avoid instability due to uncertainties and drifts of filter parameters. A change in the filter parameters, may lead to a decrease of the minimum or an increase of the maximum value of the resonance frequency, already predicted by (16), which may push it outside the stable range. Considering (16), the worst case for the $\omega_{res,min}$ occurs when all filter parameters have positive uncertainty (i.e. the actual values be higher than the designed ones), and for the $\omega_{res,max}$ it occurs when all filter parameters have negative uncertainty (i.e. the actual values be smaller than the designed ones). Assuming that the actual values of filter parameters, with a subscript '*a*', are related to the designed values as $L_a = k_L L$ and $C_a = k_C C$, then, the actual resonance frequency can be derived as

$$\omega_{res,a} = \frac{\omega_{res}}{\sqrt{k_L k_C}}. \quad (19)$$

For the given values of k_L and k_C, with the goal of achieving the zero phase margin for the worst case of parameter uncertainties, the values of the PM_{2d} and PM_{3d} can be derived using (15), (17) and (18) as

$$\begin{cases} PM_{2d} = (\sqrt{k_L k_C} - 1)\pi/2 \\ PM_{3d} = 3(1 - \sqrt{k_L k_C})\pi/2 \end{cases}. \quad (20)$$

5.4 Proposed design procedure

Two sets of limits and constraints are already presented in Sections 5.1 and 5.2. Satisfying them simultaneously results in a filter with good harmonic attenuation and sufficient stability margins, regardless of the grid impedance conditions. After choosing the limits x_1, x_2 and x_3 and the range of parameters uncertainty (k_L and k_C), according to the application requirements, the *LCL* and *LLCL* filter parameters can be calculated according to the following straightforward step-by-step procedure:

i. For both filters, the capacitor value is initially determined from the reactive power limit as

$$C_f \le \frac{x_1 P_{rated}}{\omega_0 V_g^2} \quad (21)$$

where P_{rated} is the rated power and V_g is the rms value of the grid voltage. The second limit for the capacitor in the case of the *LCL* filter is obtained by removing L_1 from (11) and (17)

$$C_f \le \frac{8x_2 I_{P,rated}}{T_s V_{dc} \omega_{min}^2} \quad (22)$$

and in the case of the *LLCL* filter and with the extra assumption that the filter zero is exactly located at the first sideband, i.e. $1/(L_f C_f)^{1/2} = \omega_s$, we have

$$C_f \le \frac{8x_2 I_{P,rated}}{T_s V_{dc}} \left(\frac{1}{\omega_{min}^2} - \frac{1}{\omega_s^2}\right). \quad (23)$$

Hence, the minimum of (21) and (22) determines the C_f value for the *LCL* and the minimum of (21) and (23) determines the C_f value for the *LLCL* filter.

ii. In the *LLCL* filter, the first sideband is extremely attenuated by selecting the L_f value as

$$L_f = \frac{1}{C_f \omega_s^2}. \quad (24)$$

iii. With the calculated values for C_f and L_f, the value of L_1 can be determined using (17) as:

$$L_1 = \frac{1}{C_f \omega_{min}^2} - L_f. \quad (25)$$

It should be noted that the ripple limit on the converter side current is considered in selection of C_f, therefore with this value for L_1 the ripple limit is also satisfied.

iv. The value of L_2 should be determined to achieve a high attenuation of grid current harmonics based on the standards and at the same time obtain a guaranteed stability. Therefore, (4) and (12) are combined to provide a limit for the grid current attenuation for the *LCL* and the *LLCL* filters, presented in (26) and (27), respectively. Since the worst case of harmonic attenuation occurs in a stiff grid with $L_g = 0$, the following results are calculated with the assumption that $L_g = 0$.

$$L_2 \ge \left(\frac{V_{sb1,\,max}}{L_1 C_f \omega_s^3 x_3 I_{P,rated}}\right) \quad (26)$$

$$L_2 \ge \left(\frac{V_{sb2,\,max}}{2\omega_s x_3 I_{P,rated}} - L_1\right) L_f/(L_1+L_f) \quad (27)$$

The values of $V_{sb1,max}$ and $V_{sb2,max}$ can be determined from (2) or Fig. 2 for the expected range of M_a.

From the stability point of view, the limit on the value of L_2 is achieved using (18) as

$$L_2 \ge \frac{L_1(1 - L_f C_f \omega_{max}^2)}{(L_1+L_f)C_f \omega_{max}^2 - 1}. \quad (28)$$

Again for the *LCL* filter, one must replace $L_f = 0$. Hence, the maximum of (26) and (28) determines the L_2 value for the *LCL*

Table 1 Designed filter example

Filter type	Filter parameters				Design limits and constraints				
	L_1, μH	L_2, μH	C_f, μF	L_f, μH	PM_2, deg	PM_3, deg	x_1, %	x_2, %	x_3, %
LCL	570	940	4	–	23	127	2.03	27.9	0.3
LLCL	540	210	4	25	23	68	2.03	29.2	0.23

and the maximum of (27) and (28) determines the L_2 value for the *LLCL* filter.

Fig. 5*a* summarises the four step design algorithm for the *LCL* and the *LLCL* filters.

5.5 Design example

The proposed step-by-step design procedure for a single phase converter with $V_g = 220\ V_{rms}/50$ Hz, $V_{dc} = 388$ V ($M_a = 0.8$), $P_{rated} = 3$ kW and $f_c = 8$ kHz ($f_s = 2f_c$) is performed in the following and the results are summarised in Fig. 5*b*. Choosing the value of parameter uncertainties depends on the type of used capacitors and inductors. Here, the deviation of ±30% and ±20% is considered for inductances and capacitors, respectively (i.e. $0.7 < k_L < 1.3$ and $0.8 < k_C < 1.2$). Therefore, the proper stability margins can be calculated from (20) as $PM_{2d} = 23°$ and $PM_{3d} = 68°$.

i. With the reactive power limit of $x_1 = 5\%$, the capacitor should be <9.86 μF and with the current ripple limit of $x_2 = 30\%$, the maximum allowed value is 4.3 μF for the *LCL* and 4.1 μF for the *LLCL* filter. In each case, the lower value considering the available capacitors should be chosen. Therefore, the selected values are 4 μF for both *LCL* and the *LLCL* filter.
ii. With the chosen value for the capacitor of the *LLCL* filter, the value of L_f is calculated from (24) as 25 μH.
iii. The value of L_1 is calculated from (25) as 570 and 540 μH for the *LCL* and the *LLCL* filter, respectively.
iv. The limit on the value of L_2 is calculated from (26) and (27). With a dc link voltage of 388 V, which means $M_a \geq 0.8$ (considering the grid impedance volt-drop), the maximum value of the converter voltage for the first and the second sidebands is determined from Fig. 2 as $0.32V_{dc}$ and $0.12V_{dc}$, respectively. Thus the value of L_2 is calculated as 940 and 150 μH, for the *LCL* and the *LLCL* filter, respectively. Furthermore, the value of L_2 is calculated from (28) as 260 and 210 μH, for the *LCL* and the *LLCL* filter, respectively. Hence, the maximum value for L_2 is chosen as 940 and 210 μH, for the *LCL* and the *LLCL* filter, respectively.

The designed filter parameters and the resultant limits and constraints are summarised in Table 1. As expected, the achieved total inductance value for the *LCL* filter is higher than the *LLCL* filter. For both filters, the C_f value is determined by the stability constraint PM_{2d}. The L_2 value is determined by the stability constraint PM_{3d} for the *LLCL* filter and by the harmonics attenuation limit (x_3) for the *LCL* filter.

6 Experimental verification

To confirm the theoretical achievements, a 3 kW single phase VSC is constructed with the filter parameters already calculated in the previous section. The control algorithm is implemented on a TMS320F28335 floating point digital signal controller from Texas Instruments.

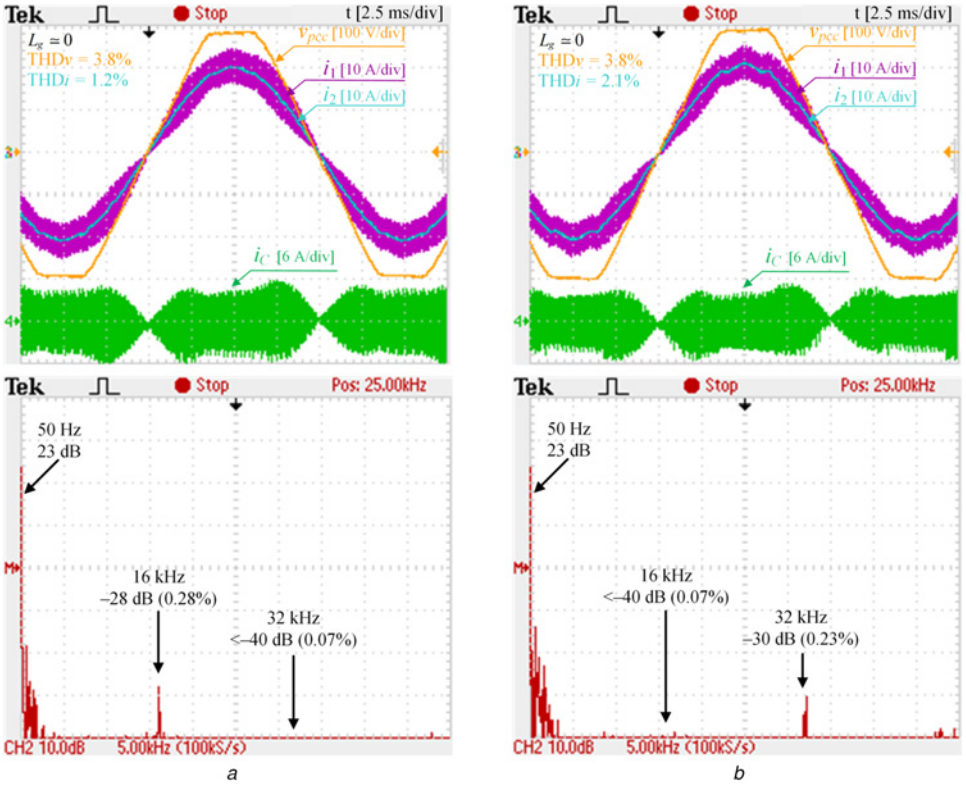

Fig. 6 *Steady state waveforms and grid current harmonic spectrum with* $L_g \simeq 0$
a LCL filter
b LLCL filter

IET Power Electron., 2016, Vol. 9, Iss. 9, pp. 1971–1978

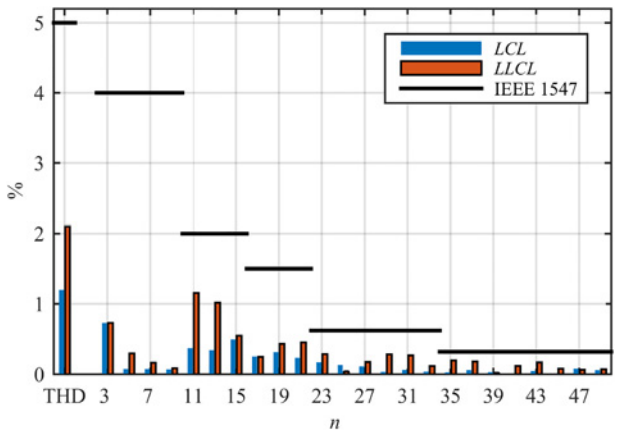

Fig. 7 *Low frequency harmonics of grid current compared with IEEE 1547 limits*

For both *LCL* and *LLCL* filters, the current controller parameters are calculated from (8)–(10), with a desired phase margin of $PM_{1d} = \pi/3$ as: $\omega_{gc1} = 5.58$ krad/s, $k_p = 8.4$ (*LCL*)/4.2 (*LLCL*) and $k_r = 940$ (*LCL*)/470 (*LLCL*). Besides the fundamental component, the set of harmonics to be regulated are selected as $n = 3$, 5, 7 and 9, based on the grid dominant harmonics. The PR controller is discretised by the impulse invariant method [31].

6.1 Steady state performance

Fig. 6 shows the steady state performance of the converter with both designed filters and $L_g \simeq 0$. Although the grid voltage is highly polluted with a THD$v = 3.8\%$, the injected current is highly sinusoidal with a THDi of about 1.2% (*LCL*) and 2.1% (*LLCL*). These results indicate that the filter parameters, as well as the current controller are designed correctly. The spectra of grid current for both filters confirm adequate switching harmonic attenuation according to design constraints. The amplitude of the dominant switching harmonic for the *LCL* filter (at the first sideband) and the *LLCL* filter (at the second sideband) is 0.28 and 0.23%, respectively, which both meet the IEEE–1547 standard requirements.

The low frequency spectra (zoomed view of Fig. 6 for $n < 50$), compared with the IEEE 1547 limits are shown in Fig. 7. As it can be seen, both filters successfully meet the IEEE 1547 standard limits. The low frequency harmonics appeared in the grid current are mainly due to the grid voltage background harmonics and the non-idealities of the real system, such as the switching dead times and the inductor core non-linearity and saturation. These

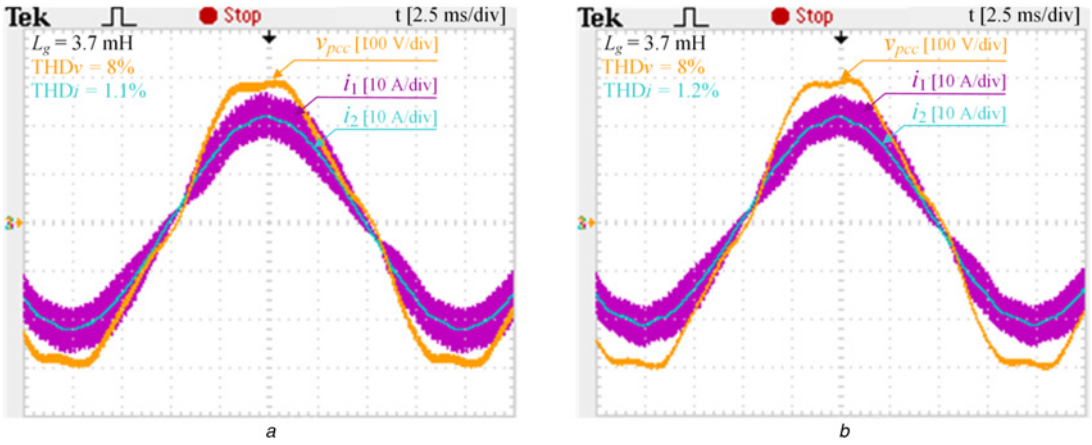

Fig. 8 *Steady state waveforms with $L_g = 3.7$ mH*

a LCL filter
b LLCL filter

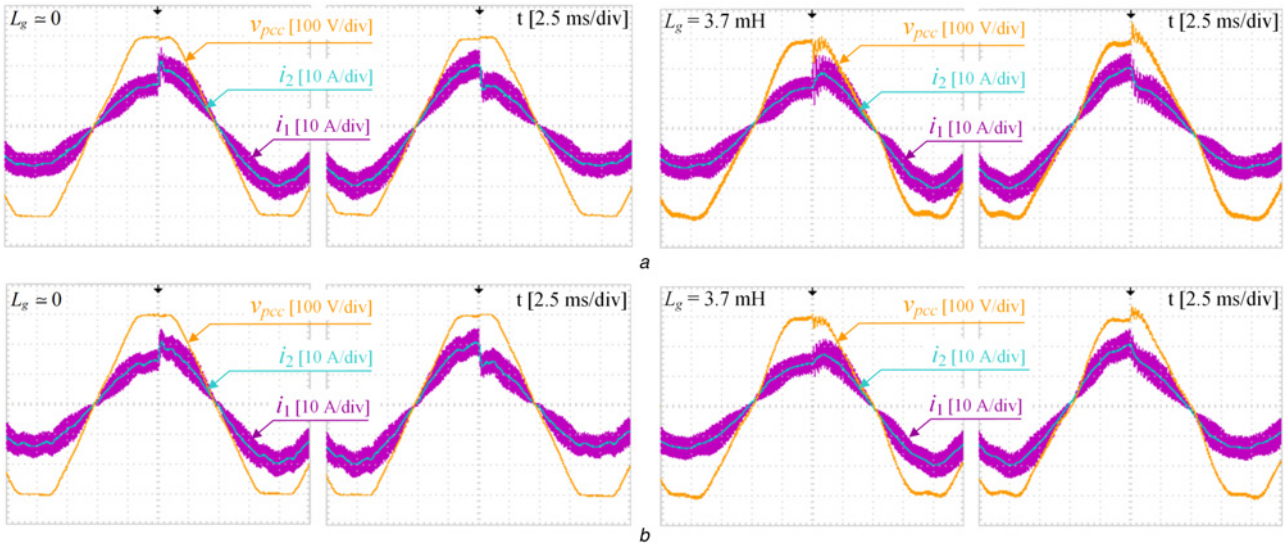

Fig. 9 *Dynamic performance in response to step changes in the reference active power from 2 to 3 kW and vice versa with $L_g \simeq 0$ and $L_g = 3.7$ mH*

a LCL filter
b LLCL filter

harmonics are attenuated primarily by the inductors in the filter structure. The harmonic compensation network in the current controller can also improve the results. It should be noted that, the higher magnitude of the low frequency harmonics and consequently higher value for THD*i* of the *LLCL* filter compared with the *LCL* one is mainly due to the lower total inductance ($L = L_1 + L_2$) of the *LLCL* filter, which makes the converter performance, in terms of the quality of the currents, more susceptible to non-idealities of the real system. Obviously, this effect decreases in presence of a higher grid impedance value and as it can be seen in Fig. 8, in such a situation, $L_g = 3.7$ mH, almost similar THD*i*s are obtained for both *LCL* and *LLCL* filters. It can be concluded that, for the filters with lower total inductance, which have the advantages of lower cost and size, the low frequency harmonic suppression level is lower and the THD*i* value is higher. Moreover, Fig. 8 confirms that both converter systems remain stable and keep their excellent performance, even in presence of a very weak grid, where a large range of impedance values and background harmonic distortions are possible.

The ripple content of the converter side current is almost equal to the capacitor current i_C. As it can be seen in Fig. 6, the maximum peak current ripple is about 6 A, which translates to 30% of the peak rated current $I_{P,rated}$.

6.2 Dynamic performance

The dynamic performance of the VSC is investigated in response to step changes in the reference active power from 2 to 3 kW and vice versa, which is shown in Fig. 9. In the case of $L_g \simeq 0$, results confirm the excellent transient response of both *LCL* and *LLCL* filtered converters, where the converter current changes almost instantaneously with a negligible oscillation. The transient performance with $L_g = 3.7$ mH shows that the converter remains stable, however the transient response is slowed down by the effect of the grid impedance. This appreciable performance can be attributed to the proper tuning of the stability margins of the converter system, PM_{1d} to PM_{3d}. It should be noted that, in all transient waveforms any oscillation corresponding to the filter resonance does not appear.

7 Conclusion

In this paper, a simple and straightforward design algorithm for the *LCL* and the *LLCL* filtered VSCs with a delay-based stabilised single-loop current controller is proposed that takes into account both filtering requirements and stability issues simultaneously. In this approach the filter parameters are designed directly and without any iteration or trial and error procedure. The constraints on the filter parameters due to the stability requirements are carefully extracted for the delay-based stabilisation method, considering the effect of grid impedance variations. As a result, the designed converters meet the filter design requirements and are also stable without the need for additional damping resistors in the filter circuit or digital filters and extra measurements in the control loop. The experimental results confirm the theoretical achievements.

8 References

1 Carrasco, J.M., Franquelo, L.G., Bialasiewicz, J.T., *et al.*: 'Power-electronic systems for the grid integration of renewable energy sources: a survey', *IEEE Trans. Ind. Electron.*, 2006, **53**, (4), pp. 1002–1016

2 Li, B., Yao, W., Hang, L., *et al.*: 'Robust proportional resonant regulator for grid-connected voltage source inverter (VSI) using direct pole placement design method', *IET Power Electron.*, 2012, **5**, (8), p. 1367

3 Peña-Alzola, R., Liserre, M., Blaabjerg, F., *et al.*: 'Analysis of the passive damping losses in LCL-filter-based grid converters', *IEEE Trans. Power Electron.*, 2013, **28**, (6), pp. 2642–2646

4 Balasubramanian, A.K., John, V.: 'Analysis and design of split-capacitor resistive-inductive passive damping for LCL filters in grid-connected inverters', *IET Power Electron.*, 2013, **6**, (9), pp. 1822–1832

5 Wu, W., Sun, Y., Huang, M., *et al.*: 'A robust passive damping method for LLCL-filter-based grid-tied inverters to minimize the effect of grid harmonic voltages', *IEEE Trans. Power Electron.*, 2014, **29**, (7), pp. 3279–3289

6 Liserre, M., Teodorescu, R., Blaabjerg, F.: 'Stability of photovoltaic and wind turbine grid-connected inverters for a large set of grid impedance values', *IEEE Trans. Power Electron.*, 2006, **21**, (1), pp. 263–272

7 Dannehl, J., Wessels, C., Fuchs, F.W.: 'Limitations of voltage-oriented PI current control of grid-connected PWM rectifiers with LCL filters', *IEEE Trans. Ind. Electron.*, 2009, **56**, (2), pp. 380–388

8 Dannehl, J., Liserre, M., Fuchs, F.W.: 'Filter-based active damping of voltage source converters with LCL filter', *IEEE Trans. Ind. Electron.*, 2011, **58**, (8), pp. 3623–3633

9 Pena-Alzola, R., Liserre, M., Blaabjerg, F., *et al.*: 'A self-commissioning notch filter for active damping in a three-phase LCL -filter-based grid-tie converter', *IEEE Trans. Power Electron.*, 2014, **29**, (12), pp. 6754–6761

10 Montagner, V.F., de Oliveira, R.C.L.F., Amaral Santini, C.L.do, *et al.*: 'Robust optimal current control for grid-connected three-phase pulse-width modulated converters', *IET Power Electron.*, 2015, **8**, (8), pp. 1490–1499

11 Pena-Alzola, R., Liserre, M., Blaabjerg, F., *et al.*: 'Systematic design of the lead-lag network method for active damping in LCL-filter based three phase converters', *IEEE Trans. Ind. Inf.*, 2014, **10**, (1), pp. 43–52

12 Tang, T., Xie, S., Xu, J.: 'Evaluations of current control in weak grid case for grid-connected LCL-filtered inverter', *IET Power Electron.*, 2013, **6**, (2), pp. 227–234

13 Xu, J., Xie, S., Tang, T.: 'Research on low-order current harmonics rejections for grid-connected LCL-filtered inverters', *IET Power Electron.*, 2014, **7**, (5), pp. 1227–1234

14 Xie, S., Xu, J., Tang, T.: 'Improved control strategy with grid-voltage feedforward for LCL-filter-based inverter connected to weak grid', *IET Power Electron.*, 2014, **7**, (10), pp. 2660–2671

15 Parker, S.G., McGrath, B.P., Holmes, D.G.: 'Regions of active damping control for LCL filters', *IEEE Trans. Ind. Appl.*, 2014, **50**, (1), pp. 424–432

16 Pan, D., Ruan, X., Bao, C., *et al.*: 'Capacitor-current-feedback active damping with reduced computation delay for improving robustness of LCL-type grid-connected inverter', *IEEE Trans. Power Electron.*, 2014, **29**, (7), pp. 3414–3427

17 Li, X., Wu, X., Geng, Y., *et al.*: 'Wide damping region for LCL-type grid-connected inverter with an improved capacitor-current-feedback method', *IEEE Trans. Power Electron.*, 2015, **30**, (9), pp. 5247–5259

18 Yin, J., Duan, S., Liu, B.: 'Stability analysis of grid-connected inverter with LCL filter adopting a digital single-loop controller with inherent damping characteristic', *IEEE Trans. Ind. Inf.*, 2013, **9**, (2), pp. 1104–1112

19 Zou, C., Member, S., Liu, B., *et al.*: 'Influence of delay on system stability and delay optimization of grid-connected inverters with LCL filter', *IEEE Trans. Ind. Inf.*, 2014, **10**, (3), pp. 1775–1784

20 Wang, J., Yan, J.D., Jiang, L., *et al.*: 'Delay-dependent stability of single-loop controlled grid-connected inverters with LCL filters', *IEEE Trans. Power Electron.*, 2016, **31**, (1), pp. 743–757

21 Lyu, Y., Lin, H., Cui, Y.: 'Stability analysis of digitally controlled LCL-type grid-connected inverter considering the delay effect', *IET Power Electron.*, 2015, **8**, (9), pp. 1651–1660

22 Liserre, M., Blaabjerg, F., Hansen, S.: 'Design and control of an LCL -filter-based three-phase active rectifier', *IEEE Trans. Ind. Appl.*, 2005, **41**, (5), pp. 1281–1291

23 Reznik, A., Simoes, M.G., Al-Durra, A., *et al.*: 'LCL Filter design and performance analysis for grid-interconnected systems', *IEEE Trans. Ind. Appl.*, 2014, **50**, (2), pp. 1225–1232

24 Wu, W., He, Y., Blaabjerg, F.: 'An LLCL power filter for single-phase grid-tied inverter', *IEEE Trans. Power Electron.*, 2012, **27**, (2), pp. 782–789

25 Xu, J., Yang, J., Ye, J., *et al.*: 'An LTCL filter for three-phase grid-connected converters', *IEEE Trans. Power Electron.*, 2014, **29**, (8), pp. 4322–4338

26 Li, F., Zhang, X., Zhu, H., *et al.*: 'An LCL-LC filter for grid-connected converter: topology, parameter, and analysis', *IEEE Trans. Power Electron.*, 2015, **30**, (9), pp. 5067–5077

27 Xiao, L., Lei, Y., Wang, Z., *et al.*: 'Optimisation of LCL filter based on closed-loop total harmonic distortion calculation model of the grid-connected inverter', *IET Power Electron.*, 2015, **8**, (6), pp. 860–868

28 'IEEE Application Guide for IEEE Std. 1547, IEEE Standard for Inter- connecting Distributed Resources With Electric Power Systems', 2008

29 Holmes, D.G., Lipo, T.A.: 'Pulse width modulation for power converters: principles and practice' (Wiley, 2003)

30 Vidal, A., Freijedo, F.D., Yepes, A.G., *et al.*: 'Assessment and optimization of the transient response of proportional-resonant current controllers for distributed power generation systems', *IEEE Trans. Ind. Electron.*, 2013, **60**, (4), pp. 1367–1383

31 Yepes, A.G., Freijedo, F.D., Doval-Gandoy, J., *et al.*: 'Effects of discretization methods on the performance of resonant controllers', *IEEE Trans. Power Electron.*, 2010, **25**, (7), pp. 1692–1712